Journal of Science and Technology, Vol. 43, No. 2 (2025), pp 78 - 90

https://dx.doi.org/10.4314/just.v43i2.6

CONTINUUM TRAFFIC MODEL ACCOUNTING FOR DRIVER BEHAVIOR AND LATERAL VISCOSITY

Gabriel Obed Fosu*, Richard Owusu, Ernest Akorly, Ellen Sarpong

Department of Mathematics, Kwame Nkrumah University of Science and Technology, Ghana

***Corresponding author: gabriel.of@knust.edu.gh**

ABSTRACT

Second-order macroscopic models consist of an LWR continuity equation and a dynamic velocity equation. From a microscopic perspective, this paper proposes a dynamic velocity equation that accounts for cautious and aggressive driving styles, as well as lateral resistance. The model's stability conditions are determined, providing important insights into traffic behavior under various conditions. The model is further solved numerically, with graphical illustrations of nonlinear traffic phenomena. Although the simulation results are based on a single-pipe scenario, the sensitivity analysis reveals a speed drop due to increased lateral resistance. This effect is evident in the shock and rarefaction wave profiles within the speed space-time and density-space-time domains.

Keywords: Traffic flow, Continuum traffic model, Viscosity rate, Driver behavior, Higher order models

INTRODUCTION

The growing number of vehicles on our roads has led to a significant rise in vehicular traffic density. The surge in the number of vehicles has not only led to an increase in traffic density, but also to rampant collisions, resulting in property damage and loss of life. Furthermore, the escalating vehicle emissions have severe consequences for air quality, human health, and the environment. Some recent publications (Ai *et al*. 2023; Qiao *et al*. 2023; Wakefield and Karni 2024) address these issues to some extent. These models have its roots from the inaugural work of Lighthill and Whitham (1955), from which the LWR model emerged. The LWR equation is also known for its characterization of speed-density profiles in the space-time domain and its realistic representation of certain macroscopic traffic features.

Though the LWR model exemplifies a myriad of vehicular flow characteristics, the model can barely describe abrupt changes in flow (Liu *et al*. 1998). Payne (1971) addressed this shortfall by introducing higher-order macroscopic models. The authors introduced an additional dynamic velocity equation and appended it with the LWR model to form a system of partial differential equation. It was later observed that Payne's model exhibited behavior similar to that of gases (Daganzo 1995), where the traffic velocity was observed to be less than the characteristic velocity. Nonetheless, other models have been developed to address this backward-traveling wave phenomenon (Fosu and Oduro 2020; Fosu, Oduro, and Caligaris 2021).

A number of these models have overlooked the heterogeneity of driver behavior (Cheng *et al*. 2017; Gidey and Kassa 2023), leading to limitations in addressing congestion and safety issues. Timid drivers tend to contribute to congestion by hesitating, while aggressive drivers exacerbate safety concerns through risky maneuvers. Additionally, lateral viscosity effects, predominantly sideway restrictions, significantly influence traffic dynamics but are often underrepresented in existing models. To effectively tackle these challenges, it is crucial to understand and accurately represent driver behavior. This includes considering the actions of assertive and timid drivers, as well as the complex interactions that take place on drivers' adjacent sides. The purpose of this paper is to formulate a macroscopic model that accurately captures the dynamics of different driving styles and incorporates restrictions from the transverse directions. This model will be derived from a microscopic equation.

Microscopic models are a variant of general traffic models with different scales of observation and analysis (Hou *et al*. 2022; Yu *et al*. 2023). Micro models explain individual-level traffic behavior and interactions. Classical categories of micro models are car-following models and cellular automata models (van Wageningen-Kessels *et al*. 2014). Car-following models were developed to explain the motion of vehicles on a single-lane road (Gazis *et al*. 1961). These models assume that drivers follow each other on a single lane without overtaking. Later, other models were introduced to realistically capture additional microscopic features. These include, but are not limited to: the optimal velocity model (OVM) (Bando 1995), the generalized force model (GFM) (Helbing and Tilch 1998), and the full velocity difference model (FVDM) (Jiang *et al*. 2001). OVM assumes that drivers aim to maintain an optimal velocity while avoiding collisions with the immediate frontal vehicle. GFM corrects the overshooting of vehicle velocity in OVM, while FVDM addresses safety in OVM by emphasizing the maintenance of a safe following distance. The OVM has also been extended to capture driver behavior (Peng *et al*. 2016), as individual drivers react differently to similar traffic situations.

Aggressive drivers may tailgate, change lanes abruptly, and speed beyond specified limits, while cautious drivers drive at or below speed limits and maintain larger following distances. In this paper, an analogous macroscopic version of Peng *et al*. model, which also takes into account lateral resistance, is presented.

IMPROVED MACROSCOPIC MODEL

The model by Gazis *et al*. (1961) is a notable introduction of microscopic traffic modeling, as stated earlier. This follow-the-leader model considers how individual vehicles on a single-lane road follow the preceding vehicle while taking into account vehicle speed and headway. This is represented by

the equation $dv_n(t + \Delta t)/dt = \lambda \Delta v$, where the velocity difference $\Delta v = v_{n+1}(t) - v_n(t)$; $v_{n+1}(t)$ and $v^n(t)$ are the respective speeds of the leading and following vehicles. Δt is the reaction time, and λ is a sensitivity coefficient.

In Gazis' model, the leading and following vehicles were observed to be close to each other at identical speed levels. Hence, another equation was developed to correct this unrealistic phenomenon (Bando 1995). The author introduced the term "optimal velocity" V . His argument was based on the idea that every car has a legal velocity, which is a function of the distance headway. Bando's optimal velocity model is given as $dv_n(t)/dt = \kappa[V(\Delta x_n(t)) - v_n(t)]$, where κ is a response parameter, $\Delta x_n(t) = x_{n+1}(t) - x_n(t)$; $x_{n+1}(t)$ and $x_n(t)$ are the respective positions of the leading and following vehicles, and V (Δx^n) is the optimal velocity of the succeeding vehicle.

With regard to the OVM, experimental investigation revealed the issue of excessive acceleration and unrealistic deceleration. Helbing and Tilch (1998) introduced a time lag of response into the optimal velocity to correct overshooting of vehicles speed with the mathematical formulation $dv_n(t)/dt = \kappa[V(\Delta x_n(t)) - v_n(t)] + \lambda \Delta v(t) H(-\Delta v(t))$.

In 1999, Treiber *et al*. noticed that if a vehicle goes faster than the one it is following, the driver of the following vehicle should not slow down, as the headway between the two vehicles will increase. This was a limitation in the generalized force model (GFM), which considered only negative velocity differences Δv, under the condition that the velocity of the following vehicle is larger than that of the leading vehicle. This led to the development of the full velocity difference model (FVDM) (Jiang *et al*. 2001), which includes both positive and negative velocity differences. This car-following model takes into account the effects of both the gap headway between two vehicles and their respective speeds. The dynamic equation for the FVDM is given by $dvn/(tdt = K[V(\Delta x_n(t)) - v_n(t)] + \lambda \Delta v_n(t)$.

Peng *et al*. (2016) extended the FVDM to incorporate timid and aggressive driver behavior as follows:

$$\frac{dv_n(t)}{dt} = \kappa\,[pV(\Delta x_n(t+\alpha\tau)) - (1-p)V(\Delta x_n(t-\alpha\tau)) - v_n(t)] + \lambda \Delta v_n(t) \quad \textbf{eqn 1}$$

where τ is the delay time, $_\kappa$ is modeled as 1/τ, $0 \le p \le 1$ is the strength of the correlation between the features of two drivers, and $_\alpha$ the driver anticipation coefficient. This model resembles the FVDM when the anticipation coefficient is zero.

As part of the derivation process, we convert this micro model to a macro model based on the following first and second order Taylor series expansions:

$$V(\Delta x_n(t+\alpha\tau)) = V(\Delta x_n(t) + \alpha\tau\Delta v_n(t)) = V(\Delta x_n(t)) + \alpha\tau\Delta v_n(t)\, V'(\Delta x_n(t)) \quad \textbf{eqn 2}$$

$$V(\Delta x_n(t-\alpha\tau)) = V(\Delta x_n(t) - \alpha\tau\Delta v_n(t)) = V(\Delta x_n(t)) - \alpha\tau\Delta v_n(t)V'(\Delta x_n(t)) \quad \textbf{eqn 3}$$

$$v(x+\Delta,t) = v(x,t) + v_x(x,t)\Delta + \frac{1}{2}v_{xx}(x,t)\Delta^2 \quad \textbf{eqn 4}$$

where Δ is the lateral distance headway. Thus, from equations (2,3), the terms in (1) simplify to:

$$pV(\Delta x_n(t+\alpha\tau)) - (1-p)V(\Delta x_n(t-\alpha\tau)) = V(\Delta x_n(t)) + (2p-1)\alpha\tau\Delta v_n(t)\, V'(\Delta x_n(t)) \quad \textbf{eqn 5}$$

Hence, equation (1) is recast as

$$\frac{dv_n(t)}{dt} = \kappa\left[V(\Delta x_n(t)) - v_n(t)\right] + \left[\lambda + (2p-1)\alpha V'(\Delta x_n(t))\right]\Delta v_n(t) \quad \textbf{eqn 6}$$

To convert the discrete variables of individual vehicles in (6) into continuous flow variables the following conversions are performed:

$$\Delta v_n(t) = v_{n+1}(t) - v_n(t) \implies v(x+\Delta,t) - v(x,t) = \Delta v_x(x,t) + \frac{1}{2}v_{xx}(x,t)\Delta^2 \quad \textbf{eqn 7}$$

$$V(\Delta x_n(t)) = v_e(k) \Rightarrow V'(\Delta x_n(t)) = -k^2 v_{e,k}(k) \quad \textbf{eqn 8}$$

$$\frac{dv_n(t)}{dt} \implies \frac{dv(x,t)}{dt} = v(x,t)v_x(x,t) + v_t(x,t) \quad \textbf{eqn 9}$$

where $v_{e,k}$ is the derivative of the equilibrium speed with respect to density. Substituting equations (7,8,9) into (6) we have:

$$vv_x + v_t = \frac{v_e(k) - v(x,t)}{\tau} + \left[\lambda - (2p-1)\alpha k^2 v_{e,k}(k)\right]\left[\Delta v_x(x,t) + \frac{1}{2}v_{xx}(x,t)\Delta^2\right] \quad \textbf{eqn 10}$$

Fosu, Adu-Sackey, *et al*. (2022) introduced the concept of lateral viscosity to explain sideway friction. This term was derived from the no-slip condition observed in fluids, and it is mathematically expressed as ϕsdvl/k, where ϕ represents the resistance rate from the sideways, and sd is the sensitivity coefficient. The term vl accounts for the variations in speed, which may be attributed to change in the utilization of different road lanes. The viscous term is appended to equation (10) to obtain the new dynamic velocity equation (11).

$$vv_x + v_t = \frac{v_e(k) - v(x,t)}{\tau} + \left[\lambda - (2p-1)\alpha k^2 v_{e,k}(k)\right]\left[\Delta v_x(x,t) + \frac{1}{2}v_{xx}(x,t)\Delta^2\right] - \frac{\varphi s_d v_l}{k} \quad \textbf{eqn 11}$$

The LWR model, together with equation (11), constitutes our new macroscopic model that incorporates driver behavior and lateral friction. That is:

$$k_t + vk_x + kv_x = 0 \quad \textbf{eqn 12}$$

$$v_t + [v - c_o\Delta]v_x = \frac{v_e(k) - v}{\tau} + \frac{\Delta^2}{2}c_o v_{xx} - \frac{\varphi s_d v_l}{k} \quad \textbf{eqn 13}$$

where $c_o = \lambda - (2p-1)\alpha k^2 v_{e,k}(k)$

QUALITATIVE AND STABILITY ANALYSIS

Putting the above into the form

$$\frac{\partial U}{\partial t} + A\frac{\partial U}{\partial x} = E \quad \textbf{eqn 14}$$

where $U = \begin{bmatrix} k \\ v \end{bmatrix}$, $A = \begin{bmatrix} v & k \\ 0 & v - c_o\Delta \end{bmatrix}$

and $E = \begin{bmatrix} 0 \\ \frac{v_e(k) - v}{\tau} + c_o\frac{\Delta^2}{2}v_{xx} - \varphi\frac{s_d}{k}v_l \end{bmatrix}$

The eigenvalues, ω of the matrix A are found by setting

$$\det(A - \omega I) = 0 \quad \textbf{eqn 15}$$

where I is the identity matrix. That is

$$\begin{vmatrix} v-\omega & k \\ 0 & v - c_o\Delta - \omega \end{vmatrix} = 0 \Rightarrow (v-\omega)(v - c_o\Delta - \omega) = 0$$

Thus $\omega 1 = v$ and $\omega 2 = v - co\Delta$. Therefore, the characteristic speed for the new continuum model is represented as:

$$\left(\frac{dx}{dt}\right)_1 = v \quad \text{and} \quad \left(\frac{dx}{dt}\right)_2 = v - c_o\Delta \quad \textbf{eqn 16}$$

The model may exhibit both isotropic and anisotropic property depending on the value of co, which heavily rely on the assertive or cautious behavior of the driver. However, when $co > 0$, the characteristic speeds are lower than or equal to macroscopic flow velocity. Thus, the new second order model will have none of its characteristics speed greater than the macroscopic flow velocity. This trait agrees with the idea that cars respond primarily to frontal stimuli.

Stability Condition

The conditions that cause non-stationary traffic flow are described in this section. A slight deviation from the steady state will be denoted by the following:

$k(x,y,t) = k_e + \delta k(x,y,t)$ and $v(x,y,t) = v_e + \delta v(x,y,t)$

This lead to the following linearized equations:

$$\frac{\partial(\delta k)}{\partial t} + v_e\frac{\partial(\delta k)}{\partial x} + k_e\frac{\partial(\delta v)}{\partial x} = 0 \quad \textbf{eqn 17}$$

$$\frac{\partial(\delta v)}{\partial t} + [v_e - c_o\Delta]\frac{\partial(\delta v)}{\partial x} = \frac{1}{\tau}[v_{e,k}(k_e)\delta k - \delta v] + c_o\frac{\Delta^2}{2}\frac{\partial^2(\delta v)}{\partial x^2} - \varphi\frac{s_d}{k_e}\frac{\partial(\delta v)}{\partial y} \quad \textbf{eqn 18}$$

Assuming that the disturbance, δk(x,t) and δv(x,t), can be replicated using the respective simple wave equations (19, 20)

$$\delta k(x,t) = k_* exp[isx + izy + (\omega - i\varphi)t] = k_* e^{\omega t}e^{i(sx+zy-\phi t)} \quad \textbf{eqn 19}$$

$\delta v(x,t) = v_* exp[isx + izy + (\omega - i\varphi)t] = v_* e^{\omega t} e^{i(sx+zy-\phi t)}$ **eqn 20**

s and $_z$ are the wave numbers, $_\phi$ is the wave speed and ω is the growth rate. A small variation in ω will lead to a jam when $\omega > 0$, a stable flow otherwise. Therefore, equations (17, 18) becomes:

$$e^{\omega t} e^{i(sx+zy-\phi t)}[k_*(\omega - \phi i) + v_e i s k_* + k_e i s v_*] = 0 \quad \textbf{eqn 21}$$

$$e^{\omega t} e^{i(sx+zy-\phi t)}[v_*(\omega - \phi i) + [v_e - c_o\Delta] i s v_* = \frac{1}{\tau}[k_* v_{e,k}(k_e) - v_*] - \varphi \frac{s_d}{k_e} i z u_* \quad \textbf{eqn 22}$$

Since $e^{\omega t}e^{i(sx+zy-\phi t)}$, equations (21, 22) is expressed in matrix form as:

$$\begin{bmatrix} \tilde{\omega} & k_e i s \\ -\frac{1}{\tau} v_{e,k}(k_e) & \tilde{\omega} + \chi + \xi i \end{bmatrix} \begin{bmatrix} k_* \\ v_* \end{bmatrix} = 0 \quad \textbf{eqn 23}$$

where $\tilde{\omega} = \omega - \tilde{\phi} i$, $\tilde{\phi} = \phi - v_e s$, $\chi = \frac{1}{\tau}$, and $\xi = (v_e - c_o\Delta)s + \varphi \frac{s_d}{k_e} z$

The characteristic polynomial derived from (23) is: $\tilde{\omega}^2 + \tilde{\omega}(\chi + \xi i) + \frac{1}{\tau} v_{e,k} k_e i s$

Using the equation $\tilde{\omega}_{1,2} = \frac{-b}{2} \pm \sqrt{\left(\frac{b}{2}\right)^2 - c}$.

The solution to the characteristic polynomial is obtained as:

$$\tilde{\omega}_{1,2} = -\frac{1}{2}\chi - \frac{1}{2}\xi i \pm \sqrt{R + i \mid I \mid} \quad \textbf{eqn 24}$$

where $R = \frac{1}{4}(\chi^2 - \xi^2)$ and $\mid I \mid = \frac{1}{2}\chi\xi + \frac{1}{\tau} v_{e,k} k_e s$

Following from Helbing and Johansson (2009):

$$\sqrt{R + \mid I \mid} = \sqrt{\frac{1}{2}\sqrt{R^2 + I^2} + R} + i\sqrt{\frac{1}{2}\sqrt{R^2 + I^2} - R} \quad \textbf{eqn 25}$$

Thus, (24) is split up into real and imaginary components. The imaginary part is denoted by Im(˜ω1,2) and the real part by Re(˜ω1,2). That implies that:

$$\mathrm{Re}(\tilde{\omega}_1) = -\frac{1}{2}\chi + \left\{\frac{1}{2}\left(\sqrt{R^2 + I^2} + R\right)\right\}^{\frac{1}{2}} \text{ and } \mathrm{Re}(\tilde{\omega}_2) = -\frac{1}{2}\chi - \left\{\frac{1}{2}\left(\sqrt{R^2 + I^2} + R\right)\right\}^{\frac{1}{2}}$$

Since Re(˜ω1) > Re(˜ω2), the instability condition for Re(˜ω1) will similarly hold for Re(˜ω2). Thence, concentrate on Re(˜ω1) in attaining the instability criterion for the proposed model. That is

$$-\frac{1}{2}\chi + \left\{\frac{1}{2}\left(\sqrt{R^2 + I^2} + R\right)\right\}^{\frac{1}{2}} \leq 0$$

Simplified as $I^2 \leq \frac{\chi^2}{4}(\chi^2 - 4R)$

Substituting the values of $_R$ and $_I$ yield:

$$\left[\frac{1}{2}\chi\xi + \frac{1}{\tau} v_{e,k} k_e s\right]^2 \leq \frac{\chi^2}{4}\left[\chi^2 - 4\left(\frac{1}{4}(\chi^2 - \xi^2)\right)\right]$$

Which is simplified as

$$\frac{1}{4}\chi^2\xi^2 + \chi\xi\frac{1}{\tau} v_{e,k} k_e s + (\frac{1}{\tau} v_{e,k} k_e s)^2 \leq \frac{1}{4}\chi^2\xi^2$$

Since $\frac{1}{\tau} v_{e,k} k_e s > 0$, the model will be stable on the condition that:

$$\chi\xi + \frac{1}{\tau} v_{e,k}(k_e) k_e s \leq 0 \quad \textbf{eqn 26}$$

This indicates that, there could be varying situations that may lead to non-stationary traffic flow. These include changes in the volume of traffic, dynamic adjustments in

driver behavior, distance headway, lateral viscosity rate, and the driver anticipation rate. For effective traffic management and to ensure the smooth flow of traffic on the roads, it is crucial to recognize and appreciate these scenarios.

NUMERICAL RESULTS AND DISCUSSION

In this section, we present the numerical solution of the proposed model. Given the coupled nature of the system of equations derived in the study, we applied the finite difference scheme, specifically utilizing the upwind technique to solve the model. The finite difference approximations corresponding to the system of equations (12) and (13) are as follows:

$$k(i+1,j) = k(i,j) + \frac{\triangle t}{\triangle x}\left(v(i,j)\left[k(i,j) - k(i+1,j)\right]\right) + \frac{\triangle t}{\triangle x}\left(vk(i,j)\left[v(i,j-1) - v(i,j)\right]\right)$$

if $v(i,j) < c_0$ **eqn 27**

$$v(i+1,j) = u(i,j) - \frac{\triangle t}{\triangle x}\left[v(i,j) - \lambda\triangle + (2p-1)\alpha k(i,j)^2 v_{e,k}\triangle\right] \times \left[v(i,j+1) - v(i,j)\right] - \frac{\triangle t}{\triangle x}\varphi\frac{s_d}{k(i,j)}v_l + \triangle t\kappa\left[v_e - v(i,j)\right] + \frac{\triangle t\triangle^2}{2}\left[\lambda - (2p-1\alpha)k(i,j)^2 v_{e,k}\right] \times \frac{\triangle t}{\triangle x^2}\left[v(i,j+1) - 2v(i,j) + v(i,j-1)\right]$$ **eqn 28**

otherwise

$$v(i+1,j) = u(i,j) - \frac{\triangle t}{\triangle x}\left[v(i,j) - \lambda\triangle + (2p-1)\alpha k(i,j)^2 v_{e,k}\triangle\right] \times \left[v(i,j) - v(i,j-1)\right] - \frac{\triangle t}{\triangle x}\varphi\frac{s_d}{k(i,j)}v_l + \triangle t\kappa\left[v_e - v(i,j)\right] + \frac{\triangle t\triangle^2}{2}\left[\lambda - (2p-1\alpha)k(i,j)^2 v_{e,k}\right] \times \frac{\triangle t}{\triangle x^2}\left[v(i,j+1) - 2v(i,j) + v(i,j-1)\right]$$ **eqn 29**

where the index j and index i represent the road section and the time interval, respectively. The above discrete problem is solved as Riemann problem with the initial conditions given as

$$k(x,0) = \begin{cases} k_l & \text{if } x \le mid_x \\ k_r & \text{if } x > mid_x \end{cases} \quad \text{and} \quad u(x,0) = \begin{cases} v_l & \text{if } x \le mid_x \\ v_r & \text{if } x > mid_x \end{cases}$$ **eqn 30**

where kl and ul represents upstream density and velocity respectively and kr and ur represents downstream density and velocity respectively.

In addition, we adopt the equilibrium speed-density relation, ve given as (Fosu, Akweittey, *et al*. 2020):

$$v_e(k) = v_m\left\{1 - exp\left[1 - exp\left(\frac{c_m}{v_m}\left(\frac{k_m}{k}\right) - 1\right)\right]\right\}$$ **eqn 31**

where v_m and k_m are respectively the free flow speed and the jam density of the lanes, and c_m is the speed of the kinematic wave under the jam density. The hypothetical parameter values used in the simulation are shown in Table 1, with the initial upstream and downstream conditions of

Table 1: Parameter values used for the simulation

Meaning	Symbol	Value	Meaning	Symbol	Value
maximum speed	*vm*	30	sensitivity coefficient	λ	0.3
delay time	τ	0.8	minimum density	ρ_{min}	0.01
inter-lane sensitivity	sd	0.37	intensity influence	p	
lateral velocity	vl	5.55	anticipation coefficient	α	0.5 0.4 0.2
maximum density	ρ_{max}	1	lateral resistance	ϕ	

density respectively set as 0.7 and 0.3.

The results of the simulation for rarefaction and shock wave are shown in figure 1 and 2 respectively. In the first case of rarefaction, the high density upstream is catching-up with the low density downstream. In figure 1-b, it is observed that, the higher density of cars built-up from the initial Reimann condition decreases with time. This phenomenon on the other hand causes cars at a standstill to move. Thus, as time increases, we observe speed of cars gradually increasing from zero at the shock front.

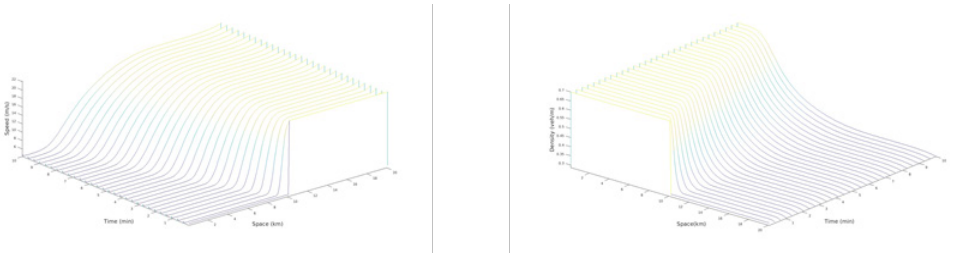

(a) Speed (b) Density

Figure 1: Rarefaction wave profiles for speed and density

Figure 2 illustrates the case where vehicles upstream with a maximum speed merges with a stopped queue of vehicles, causing the speed of the vehicle to reduce to the minimum or zero (figure 2-a). This directly affects the density of vehicles on the section of the road, causing a rise in density with time as shown in 2-b.

These results of the simulation shows a realistic highway traffic phenomenon where a high speed traffic coincide with either jammed or fairly jammed traffic. In these scenarios, the model proposed in this study can be used for traffic studies

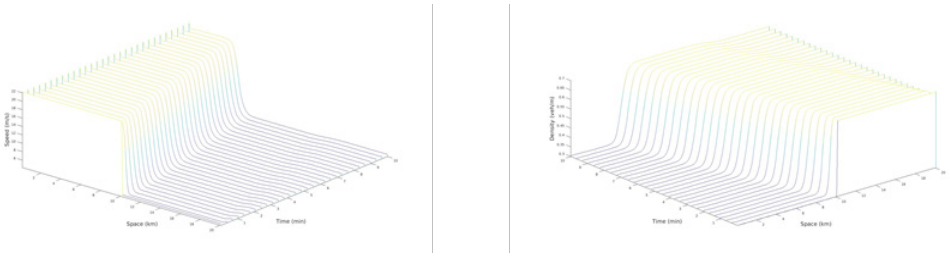

(a) Speed (b) Density

Figure 2: Shock wave profiles for speed and density

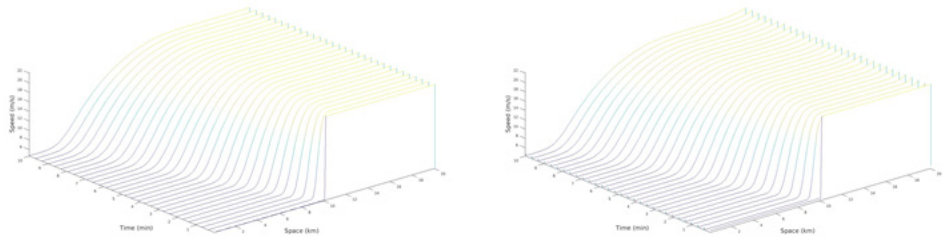

(a) φ =0.02 (b) φ =0.2

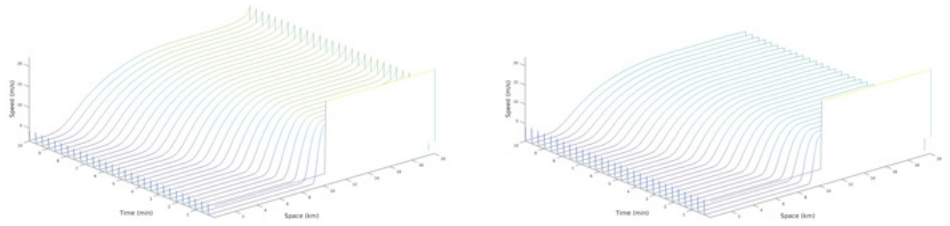

(c) φ =1.2 (d) ϕ =1.8

Figure 3: Rarefaction wave for speed at different values of ϕ

In addition to the results obtained, further analysis is carried out to ascertain the effects of lateral viscosity rate on moving vehicles. To observe the effects of the lateral viscous rate, realistic values of φ are chosen for the simulation. These values were chosen to represent variations from minimal to substantial lateral resistance, as encountered in real-world traffic scenarios. Minimal φ values represent conditions with low lateral resistance, such as open road segments where vehicles experience limited sideway friction, allowing for relatively unimpeded movement. Moderate ϕ values correspond to typical road conditions with an average level of lateral interaction, which is commonly observed in moderately congested traffic. Higher φ values simulate intense lateral resistance scenarios, such as those on busy multi-lane highways where vehicles are densely packed and subjected to significant side friction due to close proximity. Figures

3 and 4 show the effect of this parameter on speed and density respectively. It is observed that, an increasing rate of lateral viscosity had a direct influence on speed of vehicles on the road. In figure 3, increasing the value of φ decreases the speed of vehicles. For the dissolution wave case, moving vehicles tend to reduce speed as vehicles moving alongside gets closer. This phenomenon captured in this proposed model is illustrated in figure 3 which shows a reduction in speed of vehicles by increasing φ from 0.02 to 1.8.

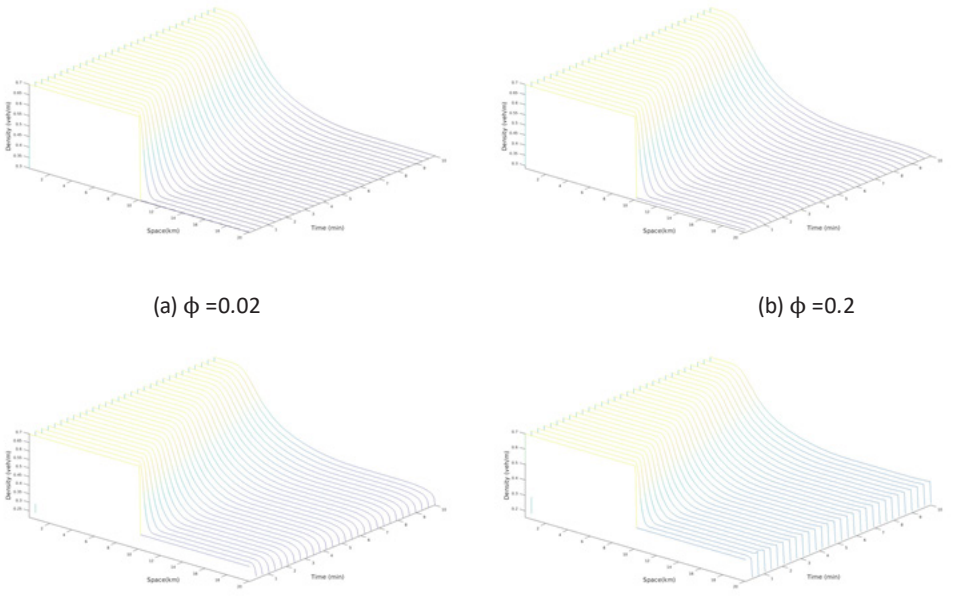

(a) ϕ =0.02 (b) ϕ =0.2

(c) ϕ =1.2 (d) ϕ =1.8

Figure 4: Rarefaction wave for density at different values of ϕ

The study further investigated the effect of lateral viscosity rate on moving vehicles merging with a stopped queue of vehicles. This parameter showed a significant effect on both speed and density. By selecting different values of this parameter, the results are shown in figures 5 and 6. In figure 5, a significant reduction in speed of vehicles joining a stopped queue of vehicles is observed as we increased the rate from 0.02 to 2.2. However, as drivers adjust after joining the queue, there is a tendency for vehicles to regain the speed though at the very minimum as shown in figures 5-c and 5-d. As the number of cars increase on the section of the road, with time, we observe high density of cars building up at the mid-section of the road.

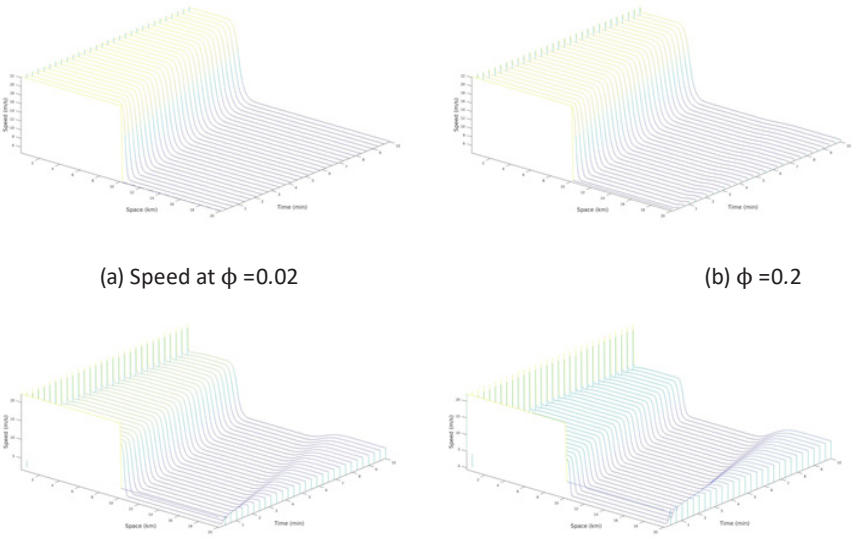

(a) Speed at ϕ =0.02 (b) ϕ =0.2

(c) ϕ =1.2 (d) ϕ =2.2

Figure 5: Shock wave for speed at different values of ϕ.

CONCLUSION

This paper presents a higher-order macroscopic traffic flow model considering lateral viscosity and the behavior of cautious and aggressive drivers. The model explores these flow characteristics, acknowledging that drivers exhibit a wide range of behaviors. Cautious drivers tend to adopt a conservative approach in responding to events on the road, while aggressive drivers demonstrate a readiness to take risks, prefer frequent lane changes, and often drive more assertively through traffic.

The model also incorporates lateral viscosity effects, recognizing how sideways friction influences driver decisions. With this approach, the model gains an added level of realism, enabling it to more accurately reflect the dynamics of real-world traffic conditions.

In addition, a mathematical derivation of the model's stability conditions is presented. This in-depth analysis offers insights into the properties and operational behavior that govern the model's functionality within the context of traffic flow dynamics. These conditions provide a

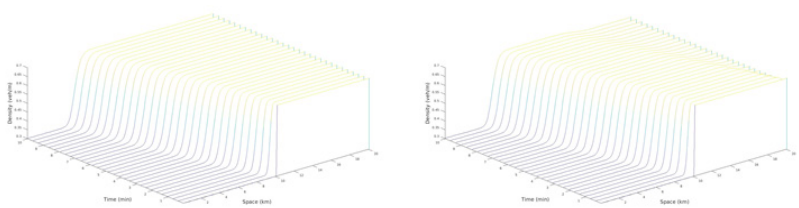

(a) ϕ =0.02 (b) ϕ =0.2

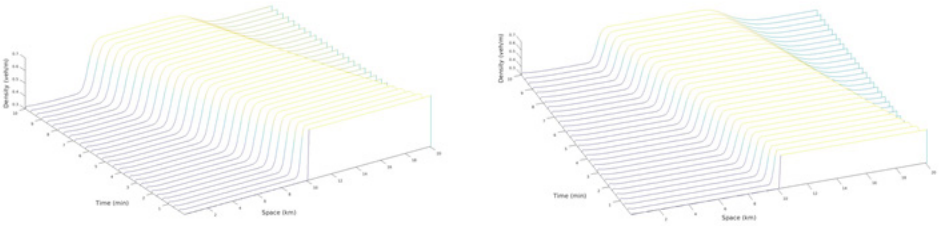

(c) ϕ =1.2 (d) ϕ =2.2

Figure 6: Shock wave for density at different values of ϕ

solid framework for understanding the range of scenarios in which the model can produce accurate and reliable predictions, equipping us with the knowledge to avoid potential pitfalls that may arise under certain parameter configurations.

Moreover, numerical simulation results for shock and rarefaction waves are presented. These visualizations capture the intricate interactions between vehicles, illustrating how their movements and interactions create various flow patterns. Shock waves emerge when rapid disturbances occur in traffic flow, and observing their development and propagation graphically offers valuable insights into how these disruptions resonate across a traffic stream. Additionally, the gradual dispersion of rarefaction waves portrays how traffic gradually resumes normal flow following periods of congestion or delay. The simulation results also indicated only minor changes in wave profiles for cautious drivers when viscosity rates varied. Conversely, for drivers exhibiting a more aggressive driving style, the impact on traffic flow was considerably greater.

REFERENCES

Ai, W. H., M. M. Wang, and D. W. Liu (2023). "Analysis of macroscopic traffic flow model considering throttle dynamics". In: *The European Physical Journal* B 96.6, p. 87.

Bando, M. (1995). "Dynamical model of traffic congestion and numerical simulation". In: *Physical Review* 51, pp. 1035–1042.

Cheng, R., H. Ge, and J. Wang (2017). "An extended continuum model accounting for the driver's timid and aggressive attributions". In: *Physics Letters. A* 381.15, pp. 1302–1312.

Daganzo, C. F. (1995). "Requiem for second-order approximations of traffic flow". In: *Transportation Research B* 29.4, pp. 277–286.

Fosu, G. O., A. Adu-Sackey, and J. Ackora-Prah (2022). "Macroscopic Analysis of The Viscous Diffusive Traffic Flow Model". In: *Mathematics in Applied Sciences and Engineering*, pp. 1–12.

Fosu, G. O., E. Akweittey, J. M. Opong, and M. E. Otoo (2020). "Vehicular traffic models for speed-density-flow relationship". In: *Journal of Mathematical Modeling* 8.3, pp. 241–255.

Fosu, G. O. and F. T. Oduro (2020). "Two dimensional anisotropic macroscopic second-order traffic flow model". In: *Journal of Applied Mathematics and Computational Mechanics* 19.2, pp. 59–71.

Fosu, G. O., F. T. Oduro, and C. Caligaris (2021). "Multilane analysis of a viscous second-order macroscopic traffic flow model". In: *SN Partial Differential Equations and Applications* 2, pp. 1–17.

Gazis, D. C., R. Herman, and R. W. Rothery (1961). "Nonlinear follow-the-leader models of traffic flow". In: *Operations research* 9.4, pp. 545–567.

Gidey, H. H. and S. M. Kassa (2023). "Extended Second-Order Multiclass Traffic Flow Model with the Relative Drag Function". In: *Available at SSRN 4374659*.

Helbing, D. and A. F. Johansson (2009). "On the Controversy around Daganzo's Requiem for and Aw-Rascle's Resurrection of Second-Order Traffic Flow Models". In: *The European Physical Journal B* 69, pp. 549–562.

Helbing, D. and B. Tilch (1998). "Generalized force model of traffic dynamics". In: *Physical review E* 58.1, p. 133.

Hou, G., S. Chen, and Y. Bao (2022). "Development of travel time functions for disrupted urban arterials with microscopic traffic simulation". In: *Physica A: Statistical Mechanics and its Applications* 593, p. 126961.

Jiang, R., Q. Wu, and Z. Zhu (2001). "Full velocity difference model for a car-following theory". In: *Physical Review E* 64.1, p. 017101.

Lighthill, M. J. and G. B. Whitham (1955). "On kinematic waves II: A theory of traffic flow on long crowded roads," In: *Proceedings of the Royal Society of London. Series A Mathematical and Physical Sciences* 229.1178, pp. 317–345.

Liu, G., A. S. Lyrintzis, and P. G. Michalopoulos (1998). "Improved high-order model for freeway traffic flow". In: *Transportation Research Record* 1644.1, pp. 37–46.

Payne, H. J. (1971). "Models of freeway traffic and control". In: *In: G. A. Bekey (ed.) Mathematical Models of Public Systems (Simulation Council, La Jolla, CA)* 1, pp. 51–61.

Peng, G., H. He, and W.-Z. Lu (2016). "A new car-following model with the consideration of incorporating timid and aggressive driving behaviors". In: *Physica A: Statistical Mechanics and its Applications* 442, pp. 197–202.

Qiao, D., B. Dai, Z. Lin, M. Guo, X. Zhang, P. Zhang, and F. Cheng (2023). "Study on vehicle fuel consumption and exhaust emissions based on a new viscous macroscopic traffic flow model". In: *Journal of Transportation Engineering, Part A: Systems* 149.2, p. 04022137.

Treiber, M., A. Hennecke, and D. Helbing (1999). "Derivation, properties, and simulation of a gas-kinetic-based, non local traffic model". In: *Physical Review E* 59.1, p. 239.

van Wageningen-Kessels, F., H. van Lint, K. Vuik, and S. Hoogendoorn (2014). "Genealogy of traffic flow models". In: *EURO Journal on Transportation and Logistic*.

Wakefield, J.P., Karni, S. (2024). Traffic Flow Models with Noise. In: Parés, C., Castro, M.J., Morales de Luna, T., Muñoz-Ruiz, M.L. (eds) Hyperbolic Problems: Theory, Numerics, Applications. Volume II. HYP 2022. SEMA SIMAI Springer Series, vol 35. Springer.

Yu, S., Y. Chen, L. Song, Z. Xuan, and Y. Li (2023). "Modelling and mitigating secondary crash risk for serial tunnels on freeway via lighting-related microscopic traffic model with inter-lane dependency". In: *International journal of environmental research and public health* 20.4, p. 3066.